Intensification characteristics of hydroclimatic extremes in the Asia monsoon region under 1.5 and 2.0 °C of global warming

Jeong-Bae Kim[1], Deg-Hyo Bae[1]

[1] Department of Civil and Environmental Engineering, Sejong University, Seoul, 05006, Korea

5 *Correspondence to*: Deg-Hyo Bae (dhbae@sejong.ac.kr)

Abstract. The changes in hydroclimatic extremes are assessed over the Asia monsoon region under 1.5 and 2.0 °C warming targets of global mean temperature above preindustrial levels based on a representative concentration pathway (RCP) 4.5 scenario. The subregions in this domain are defined by the Köppen climate classification method to identify regional climate characteristics. The change patterns of long-term hydroclimatic mean and hydroclimatic extreme among subregions are

10 compared based on the multimodel ensemble (MME) of selected five global climate models (GCMs). Each GCM is bias corrected and then used as a meteorological forcing for a hydrological model. To simulate how the hydrologic system responds to 1.5 and 2.0 °C global warming targets, we select the variable infiltration capacity (VIC) model. The results of temperature extremes show significant change patterns over all climate zones. As the globe warms, the increasing warm extremes and the decreasing cold extremes with a high robustness occur more frequently over Asia. Meanwhile, changes in precipitation and

15 runoff averages (and low runoff extremes) show large spatial variations in change patterns with little robustness based on intermodel agreement. Global warming is expected to significantly intensify maximum precipitation extremes in all climate zones. Regardless of regional climate characteristics, this behavior is expected to be enhanced under 2.0 °C compare to 1.5 °C warming scenario and cause the likelihood of flood risk. The spatial extent and magnitude of change patterns in runoff are modulated by those of change patterns in precipitation. More importantly, an extra 0.5 °C of global warming also leads to

20 amplified change signals and more robust change patterns in hydroclimatic extremes, especially in cold (and polar) climate zones. The results of this study demonstrate that the clear changes in regional hydroclimatic extremes under warmer conditions over Asia, and hydroclimatic sensitivities differ based on regional climate characteristics.

1 Introduction

Asia is highly vulnerable to natural disasters, such as floods and droughts, due to its large population and monsoon climate

25 (International Panel on Climate Change (IPCC), 2013). The climate system in this region has changed result from the global warming and consequently increased the frequency and intensity of natural disasters related to climate (e.g., heatwaves, heavy precipitation, floods). Moreover, further increases of atmospheric greenhouse gases (GHGs) will enhance the global warming and cause the changes in temporal and spatial patterns of both climate averages and climate extremes at the regional scale (e.g., Trenberth, 2011; Chevuturi et al., 2018). Therefore, it is essential to simulate reliable future climate changes to understand

30 their impacts on climate extremes as well as on hydrology over Asia region.

The general approach for climate change impact assessment is to project future climate changes based on scenarios using global climate models (GCMs) and then to downscale climate projections to a regional scale, finally to assess the impacts on interest areas (e.g., climate, water resources and climate extremes). According to this process, many previous studies on changes in climatic elements and hydrologic variables under global warming have been analyzed based on certain 30-year

35 future periods, which are arbitrarily defined by a particular time span (i.e., near future, mid-century and distance future period) compared with a 30-year reference period (e.g., Bae et al., 2011; Jung et al., 2013). The studies have shown a hydroclimate response in future periods, but there is a limitation to understanding how the response is regulated on the degree of current global temperature rise or more feasible future conditions.

To avoid catastrophic consequences induced by climate change, the consensus on the target warming levels of global mean
40   temperature was achieved in the 2015 Paris Agreement by parties to the United Nations Framework Convention on Climate
Change (UNFCCC). The aim of this agreement is to keep the increase of global mean temperature far below 2.0 ℃ above
preindustrial (PI) levels and seek targets to keep the increase to 1.5 ℃ above PI levels (UNFCCC, 2015). Therefore, recent
studies have pay attention to the impacts of certain target warming levels (i.e., 1.5 and 2.0 ℃) on climate variables and to the
benefits of reducing an extra 0.5 ℃ of global warming (IPCC, 2018). The studies show robust and significant impacts of an
45   extra 0.5 ℃ of global warming on climate extremes (Syllar et al., 2018 and Harrington and Otto, 2018 for Europe) and on
hydrological variables-related extremes (King et al., 2017; Marx et al., 2018 for Europe; Diedhiou et al., 2018 and Nkemelang
et al., 2018 for Africa; Wang et al., 2019; Kharin et al., 2018 for global). These findings indicate the necessity of understanding
global warming impacts on climate (and hydroclimatic) extremes and the need to find countermeasures to reduce the potential
damage that can be induced under the increases in global mean temperature.

50   For Asia region, there are several studies about the global warming impacts on climate extremes at the continental scale.
Chevuturi et al. (2018) evaluated daily extremes in temperature and precipitation (i.e., the 99th percentile on a daily basis in
nature) over the Asian-Australian monsoon region and suggested that the frequency and persistence of extremes increases.
Bhowmick et al. (2019) analyzed extreme precipitation (99th percentile) changes across South Asian region for each 0.5 ℃
increase of global mean temperature and showed a significant changes in extreme events of precipitation over the Indian region.
55   Ge et al. (2019) showed significant changes in precipitation extremes across Southeast Asia at increases between 1.5 and 2.0 ℃,
showing the responses of extreme events on the 0.5 ℃ increase. On the other hand, previous studies suggested that global
warming would lead to significant extreme climate events (e.g., temperature, precipitation), especially in a 2.0 ℃ compared
to a 1.5 ℃ warming (Li et al., 2018; Chen et al., 2018) focused on the country scale. The studies also indicated more increases
in precipitation intensity and an enhanced impacts on extreme precipitation in the warmer world (Zhou et al., 2018; Sui et al.,
60   2018 for China).

In fact, climate conditions of Asia are influenced by a large-scale climate system. However, only few studies have assessed
extreme hydroclimatic responses under global mean temperature increases at the continental scale over Asia. The studies
conducted at the country and continental scale in Asia mainly address climate extremes, so there are limitations to examining
the hydroclimatic (e.g., precipitation and runoff) extreme responses under target global warming levels. On the other hand,
65   some studies on hydroclimatic extreme responses under global warming have been conducted at the basin scale (Zhang et al.,
2019; Wen et al., 2019; Jiao and Yuan, 2019), suggesting the increases in their intensity as well as frequency.

In the study, we assess changes in climate (and hydroclimate) extremes corresponding to 1.5 and 2.0 ℃ of target warming
with a focus on the broad continental-scale climate zones of the Asian monsoon region (Figure 1), as delineated by Bae et al.
(2013). Since climate extreme events are an inherent part of climate, we classify the subregions in the Asian monsoon region
70   considering regional climate characteristics to understand the change behavior of climate (and hydroclimate) extremes under
global warming. To simulate the climate for historical and future period, the five global climate models (GCMs), which is
conducted on the Coupled Model Intercomparison Project phase 5 (CMIP5; Taylor et al., 2012) are selected by applying the
evaluation procedure (Kim et al., 2019). Then, a reference 30-year period and two future 30-year periods of individual GCM
projections are defined under 0.48, 1.5 and 2.0 ℃ warming targets since PI levels (1861-1890) based on the time sampling
75   method. Selected five GCM projections are spatially disaggregated and used as a meteorological forcing to run the variable
infiltration capacity (VIC) hydrological model. This forcing data (e.g., precipitation, maximum temperature and minimum
temperature variables) at the daily time is statistically bias corrected using quantile mapping method. The future changes in
hydroclimatic mean and extremes corresponding to 1.5 and 2.0 ℃ of warming target conditions are spatially analyzed
according to identified subregions based on the climate zone. We focus on the hydroclimatic extreme responses to temperature,
80   precipitation, and runoff variation under global warming targets (i.e., 1.5 and 2.0 ℃) using the extreme indices.

As far as we know, relatively few studies have suggested the impacts of global warming on extreme hydroclimatic variables-related responses considering regional climate in Asia. In this study, we suggest the results based on the multimodel ensemble mean (MME) which is derived from five GCM projections including intermodal agreement to consider a reliability of future projections. This study provides scientific information for policy makers on identifying regional change patterns in extremes

85   to recognize the impacts of anthropogenically induced warming.

2 Materials and methodology

2.1 Study area and climate zone classification

The study area covers the Asian monsoon region with latitudes ranging from 9.75˚ S to 54.75˚ N and longitudes ranging from 60.25˚ E to 149.75˚ E, as shown in Figure 1. This region is subdivided based on the regional precipitation and temperature

90   patterns using Köppen's climate classification method (Köppen, 1936). Each subregion is categorized as a mainly tropical climate (A), arid climate (B), warm temperate climate (C), snow climate (D) and polar climate (E) according to climate boundary conditions, which are based on threshold values of monthly temperature and precipitation (e.g., temperatures for climate zones A, C, D and E; and moisture availability would be required for plant growing for climate zone B). Due to the method's simplicity with ecologically meaningful classifications, it has been widely used in many studies, such as climate

95   change impact assessments on different climatic characteristics (Lee et al., 2015; Fernandez et al., 2017). Table 1 shows a detailed description of the Köppen climate classification. To apply this method, we used long-term observations such as maximum temperature, minimum temperature and precipitation data at a monthly time scale during the 30-year historical period (January 1976-December 2005).

2.2 Climate change scenario and definition of the periods corresponding to 1.5 °C (2.0 °C) of warming

100   Reliable future projections are important sources to estimate the global warming impacts on hydroclimatic extremes (e.g., temperature, precipitation, and runoff extremes). Here, as suggested in Kim et al. (2019), we collect CMIP5 19 GCMs considering the data availability to compare each GCM's ability to represent climatological characteristics in this study area (Figure 1). We use total twelve relevant variables which are consist of the seven two-dimensional surface meteorological variables (e.g., precipitation, near-surface air mean, maximum and minimum air temperature, outgoing longwave radiation,

105   sea-level pressure, sea surface temperature) and the five three-dimensional vertical meteorological variables (e.g., air temperature, geopotential height, specific humidity, zonal wind, and meridional wind) required for a historical climate evaluation. Individual GCMs are spatially disaggregated at a 0.5° horizontal resolution based on the bilinear interpolation algorithm. The GCMs are assessed in their simulation of a historical climate compared against observations (see section 2.4), namely, climatological features of the twelve variables in the summer season (June-September) for the reference period (1976-

110   2005). The spatial correlation coefficient (SCC) and root mean square error (RMSE) between historical simulation derived from each GCM and the observations over Asian monsoon region are calculated based on individual twelve relevant variables. The performance of each GCM simulation is assessed by comparing the performance of a MME based on the scoring rule (Nyunt et al., 2012). Performance score of each GCM are allocated based on the following criteria:

1) A score of 1 : GCM that has lower RMSE and higher SCC than MME

115   2) A score of -1 : GCM that has higher RMSE and lower SCC than MME

3) A score of 0 : GCM that does satisfy only one condition.

Finally, we selected five GCMs; bcc-csm1-1-m, CanESM2, CMCC-CMS, CNRM-CM5, and NorESM1-M with the highest scores based on a result of total scores considering all variables as shown in Table S1. The information of selected GCMs are suggested in Table 2.

120 Our focus is on an understanding of changes in extreme hydroclimatic under 1.5 and 2.0 ℃ of global warming environment based on the RCP4.5 scenario, which is commonly considered as a realistic future projection. The RCP4.5 is a stabilization emission scenario with radiative forcing at approximately 4.5 W/m² in the year 2100 without ever exceeding that value (Thomson et al., 2011; Van Vuuren et al., 2011). This scenario assumes that emission mitigation policies are implemented to achieve the goal of limiting emissions and radiative forcing. Although the RCP4.5 scenario is based on a medium-low GHG

125 emission pathway, global warming climate condition under RCP4.5 impacts on hydroclimatic phenomena (Chen et al., 2017; Donnelly et al., 2017; Kim et al., 2019). It implies the need on both mitigation and adaptation plans according to global warming induced by GHG emission even under the relatively less pressing RCP scenario (e.g., RCP4.5). In this regard, the results based on RCP4.5 can provide a useful information for recognizing the impacts of global warming on extreme hydroclimatic from those expected under "business-as-usual."

130 Next, for the selected five GCMs, we determined the reference period corresponding to 0.48 ℃ and two future periods corresponding to 1.5 and 2.0 ℃ increase in global mean temperature under RCP4.5 scenario above the PI period (1861-1890). For this process, we applied the time sampling method (James et al., 2017; Sylla et al., 2018). All five GCMs reach specific warming levels in different central year and 30-year reference and future periods (Table 3). Because the individual GCMs simulate the climate based on their own physical climate system processes, warming phases of GCM are different each other

135 even in the same emissions forcing. In this study, the first time anomalies surpass 0.48 ℃, 1.5 and 2.0 ℃ above the value of PI period, it is referred as a central years for reference, two future periods, respectively. To do this, the 30-year running global-mean temperature is derived from the individual GCMs during the entire period (1880-2100). Compared to the value of the central year of PI period (1895), the temperature anomalies are calculated for the entire period. For the reference period, we select 0.48 ℃ of warming level which is derived by Sylla et al. (2018) based on the HadCRUT.4.6 data. The central year and

140 30-year periods for each GCM with 0.48, 1.5 and 2.0 ℃ of global mean temperature increases based on the RCP4.5 scenario are suggested in Table 3. Therefore, each GCM with own time period under global warming provides meteorological forcings to run the VIC hydrological model. The reference feature (denoted as REF) is derived from the MME of selected GCMs averaged over the historical period corresponding 0.48 ℃ of warming levels. And, the future 1.5 ℃ (2.0 ℃) warming feature (denoted as +1.5 ℃ and +2.0 ℃) is derived from the MME averaged over individual 30-year periods corresponding to the

145 central year surpassing 1.5 ℃ (2.0 ℃) of warming levels.

Although we select five GCMs with relatively better performances in this study area, generally, there are a lack of accuracies in simulating observed climate characteristics because all GCMs contain a substantial bias. Additionally, the quality of meteorological forcing (e.g., precipitation, temperatures) for hydrological model is more important to estimate hydrological responses to climate changes. Therefore, we use the quantile mapping method to reduce biases statistically in temperature and

150 precipitation forcings on a daily basis. This method allows for an adjustment of the whole distribution by matching the cumulative distribution function (CDF) of climate model data to the CDF of observed data, thereby, the mean, variance, and extreme values are improved. So, this method was commonly used in many climate change studies based on the climate model (MacDonald et al., 2018; Reiter et al., 2018).

2.3 Hydrological model

155 The VIC distributed hydrologic model (Liang et al., 1994; 1996) is used to simulate runoff extremes in response to the global warming. The VIC model simulates interactions between land and atmosphere as well as water balances by sharing several fundamental schemes with other land surface models at the daily or subdaily time step. Therefore, it is commonly coupled with GCM, not only on the continental scale but also on the global scale (Sheffield et al., 2009; Lee et al., 2015). We set up the VIC model at a spatial resolution of 0.5° (approximately 50 km) considering the domain scale and run the model on a daily

160 basis, which is the same as that suggested in Bae et al. (2015).

And, we collect the geophysical datasets which are required for the VIC model, for instance digital elevation model (DEM) data from the United States Geological Survey (USGS), soil data from the Food Agriculture Organization (FAO, 1998), and the land-use data from the University of Maryland (Hansen et al., 2000). The collected datasets are converted to a 0.5° grid resolution to conform to the spatial resolution of the VIC model.

165 Because runoff simulation results are depend on model parameters, calibration and verification of model parameters are important in hydrological models to obtain a reliable runoff simulation (Bae et al., 2011). Some model parameters are estimated based on geophysical datasets and river networks for gauged basins but the remaining parameters for ungauged basins are indirectly estimated by using the hydrological regionalization method (Parajka et al., 2013; Bae et al., 2015; Beck et al., 2016). We apply hydrological regionalization method by transferring parameters obtained from gauged region into an ungauged

170 region based on the assumption that two basins with analogous climate feature (e.g., based on the classified climate zone) exhibit similar hydrological responses. In this study, the model parameters are estimated based on grid runoff, therefore, assumption is that the time delay described by channel routing scheme is not significant considering horizontal grid resolution. Due to this reason, one limitation to note is that it may have an influence on the uncertainty in simulating in the runoff. The VIC model covers the Asia monsoon region with a 0.5° of grid system (Figure 1). We draw on the VIC model results based

175 on a 0.5° implementation for the Asian monsoon region. In this study, the simulated runoff is driven by observational meteorological forcing for the historical period (1950-2005) to compare the historical runoff records obtained from Global Runoff Data Centre (GRDC). Some results of parameter validation for the VIC model in six River basins (Figure S1) considering data availability of measuring records are shown in Table S2 and Figure S2, and more additional results can be found in previous study (Bae et al., 2013). Overall, validation results suggest that the VIC model is able to simulate runoff

180 acceptably.

2.4 Observational datasets

Observational meteorological datasets (1950-2005) at a daily timescale are required as input variables to the VIC model and for validating the performance of the GCM simulations. We collect the precipitation data from APHRODITE (Yatagai et al., 2012). And, the maximum and minimum temperature data and wind speed data are extracted from gridded forcing datasets,

185 which are suggested by the University of Washington (Adam and Lettenmaier, 2003; Adam et al., 2006). In addition, we collect the reanalysis data from the Coupled European Centre for Medium-Range Weather Forecasts (ECMWF) reAnalysis system-20C (CERA-20C) (Laloyaux et al., 2018) at a monthly time scale. And, it is used to evaluate the performance of the GCM simulations to select the best-performing GCMs. We extract the climate variables from CERA-20C and interpolate them to the same grid system of GCMs. These observational and reanalysis data are gridded at a 0.5° spatial resolution.

190 2.5 Extreme indices

Fixed-threshold indices are needed as extreme indices for the purpose of comparing changes in hydroclimatic extremes among different climate regions under target global warming conditions. We select the four temperature extreme indices, six precipitation extreme indices, and three extreme runoff indices for extreme climate and runoff analyses (Table 4). The extreme indices used in this study are widely accepted for extreme analyses (Dosio and Fischer, 2018). For changes in temperature

195 extremes, Tropical days (TR), Frost days (FD), Warm nights (TN90p), and Cold nights (TN10p) are calculated by daily minimum temperature data in the reference period and two future periods. Summer days (SU), Ice days (ID), Warm days (TX90p), and Cold days (TX10p) are calculated by daily maximum temperature data. The extreme indices associated with daily precipitation are very wet day precipitation (P95), extreme wet day precipitation (P99), annual maximum precipitation (PX1D), and maximum precipitation over 2, 3, and 5 consecutive days (PX2D, PX3D, and PX5D). Finally, the variables

200 associated with extreme runoff, as suggested by Nandintsetseg et al. (2007), are 7 and 30 consecutive days of minimum runoff

(DWF07 and DWF30) and annual maximum runoff (MDF). Table 4 describes the detailed information of total extreme indices used in this study.

3 Results

3.1 Classification of climate zone and validation of reference simulation

Figure 1 shows the classified climate zones by applying Köppen's climate classification method. The Asia monsoon region was divided into twelve climate zones. The tropical climate zone (A) spreads over Indonesia, Malaysia, the Philippines, and Thailand, with low latitudes (Aw), the northwestern part of India, Myanmar (Am; located between Af and Aw), the northern part of Indonesia, India, Vietnam, Thailand, and Myanmar (Aw; located between 9° N and 25° N). The arid climate zone (B) spreads over northwestern China, some parts of Mongolia, India, Pakistan, and Afghanistan (BS), as well as northern China, southern Mongolia, Pakistan, and Kazakhstan (BW). The warm temperature climate zone (C) appeared in central and northern India, and some parts of Afghanistan (Cs); the south and eastern parts of China, northern part of India, Vietnam, Thailand, Myanmar, and southern part of South Korea (Cw); and most of the southeastern part of China, costal region of South Korea, and southern part of Japan (Cf). The cold climate zone (D) spreads over the northern part of Afghanistan (Ds), northeastern China, and most of the inland region in the high latitudes (Dw, Df) above 38° N. The tundra climate zone (ET) appears on the Tibetan Plateau and the Himalayan Mountain region. The largest number of Asian monsoon region grid points are in the D zone followed by the B, C, A, and E zones, and the ratio for each region are suggested in Table 1.

Prior to the assessment of the global warming influence on extreme hydroclimate in the Asia monsoon region based on the GCM projections, the bias-corrected GCMs are validated whether GCM simulations can adequately represent the historical climatological characteristics noted in the observed changes. The precipitation data obtained from the MME of multi GCMs and APHRODITE at the grid points in the study area (see Figure 1) for long-term period (1950-2005). Hereinafter, the results based on the MME of the selected five GCMs and from APHRODITE are referred as MME and OBS, respectively.

Figure 2 indicates a spatial distribution of the climatological annual mean precipitation (hereafter referred to as PANN) and climatological annual maximum precipitation (hereafter referred to as PX1D) of OBS and MME (1976-2005). The MME properly captures both the spatial pattern and magnitude PANN as well as PX1D (Figure 2a, b). Despite the similarity in the PX1D values between OBS and MME, MME shows a tendency to slightly overestimate the OBS PX1D for southeast Asia and southeast China (for a PX1D range of 45-90 mm/day), as presented in Figure 2b. Although there is a deficiency between the OBS and MME precipitation values, the MME, which is derived from the bias corrected GCMs reflects the OBS characteristics of both PANN and PX1D. The MME results shows reasonable historical climate simulation with implications for the reliability of the hydrological response on the climate forcing derived from MME.

3.2 Future projections of temperature extremes under 1.5 and 2.0 °C of warming

We examine the future changes in temperature extracted from the MME according to global warming. We calculated the changes in extreme temperature indices under two global warming scenarios on the basis of relative concepts which is introduced by the difference between the reference period (REF) and the each target condition (+1.5 °C and +2.0 °C). We identify the regions with 100 % of intermodel agreement on the change sign, which shows a high degree of consistency of results across the different GCMs.

Figure 3 shows the relative changes in cold extreme indices (FD, ID) and warm extreme indices (SU, TR), which are derived from MME between warming conditions (i.e., 1.5 and 2.0 °C) and REF over Asia. For temperature change, the totally consistent patterns show a decreasing change signal of cold extremes (FD, ID) and an increasing change signal of warm extremes (SU, TR) with 5 out of 5 model agreements under the both 1.5 and 2.0 °C warming conditions. The change patterns

Hydrology and
Earth System
Sciences
Discussions
Open Access
EGU

in the temperature extreme indices over Asia are amplified under 2.0 ℃ rather than under 1.5 ℃, as suggested in a previous study (e.g., Chevuturi et al., 2018; Sui et al., 2018). Especially, cold extreme indices (FD, ID) exhibit large decreases in the mid-latitude region (above 25° N) compared to the low-latitude region (below 25° N). Meanwhile, tropical nights (TR) show large increases in the low-latitude region (below 25° N). The increase in summer days (SU) is dominant in most regions except

245 for the low-latitude region (below 25° N). However, some areas show no changes in certain indices because the changes in temperature extreme indices are estimated based on fixed-threshold criteria (Dong et al., 2018). For example, low-latitude regions (below 25° N; A zones) with high maximum and minimum temperatures do not represent changes in cold extreme indices (Figure 3a, b) or warm extreme indices (Figure 3d). On the other hand, the ET zone and high-latitude region (above 40°N) with low temperatures do not show changes in the SU or TR, respectively (Figure 3c, d). This is because in this region,

250 even though the global mean temperature is increased by 1.5 ℃ (2.0 ℃) compare to the PI levels, the daily temperature of some days is not large enough to reach the criterion of warm extreme indices (i.e., TN exceeding 20 ℃).

Figure 4 shows the area-average of changes in cold and warm extreme indices, which is derived from the result shown in Figure 3. The area-averaged value is derived from the averaged values over all grid points included in each classified climate zone. The change in FD over the Asia (within 12 climate zones) represents the largest decrease of approximately -9.0 % (-

255 20.1~0.0 %) at 1.5 ℃ condition and -14.1 % (-32.4~0.0 %) at 2.0 ℃ condition. The change in ID also decreases by approximately -5.7 % (-16.3~0.0 %) at 1.5 ℃ condition and -9.0 % (-26.3~0.0 %) at 2.0 ℃ condition. A large reduction in both FD and ID is shown in the cold climate zones (Ds, Dw, and Df) and polar climate zones (ET) with lower temperature records than other climate zones. In contrast, the change in TR over the Asia including 12 climate zones represents the largest increase of approximately 9.6 % (0.0~31.7 %) at 1.5 ℃ condition and 20.6 % (0.0~45.3 %) at 2.0 ℃ condition, respectively.

260 Similarly, the change in SU is also increased by approximately 9.6 % (0.2~15.0 %) at 1.5 ℃ condition and 15.1 % (0.4~31.4 %) at 2.0 ℃ condition. The large magnitudes of change in TR, both TR and SU, are shown in the tropical zones (Af, Am, and Aw) and in the warm temperature climate zones (Cs, Cw, and Cf), respectively.

Understanding the change behavior of daily temperature is necessary for detecting a linkage to extreme temperature events. We calculate the relative changes in frequency of both daily maximum and daily minimum temperatures between individual

265 warming conditions (1.5 and 2.0 ℃) and the REF period based on the initial percentile range (e.g., 10th, 50th, and 90th-percentile values in the REF period). Figure 5 represent the redistribution of the low-percentile and high-percentile temperatures to the change in whole temperature events under 1.5 and 2.0 of warmer worlds over Asia, with 5 out of 5. In all climate zones, increased high-percentile temperatures (above the 50th percentile) frequently occur at the expense of reduced low-percentile temperatures (below the 50th percentile) under a warmer climate. In addition, this trend is clear in the

270 exceedance of extremes (e.g., below the 10th percentile or above the 90th percentile). Warm days (TX90P) is projected to increase by 23.0 % at 2.0 ℃ condition and an increase of 14.6 % at 1.5 ℃ condition over Asia. Moreover, warm nights (TN90P) are projected to increase by 31.2 % at 2.0 ℃ condition and an increase of 21.1 % at 1.5 ℃ condition. Conversely, cold days (TX10P) are projected to decrease by -6.7 % above PI levels on average in Asia at 2.0 ℃ condition and a decrease of -5.3 % at 1.5 ℃ condition. Cold nights (TN10P) are projected to decrease by -8.1 % at 2.0 ℃ condition and a decrease of -6.8 % at

275 1.5 ℃ condition. Overall, these change features in TN are more intense compared to those in TX (Figure 5a, c), which agrees with previous results (IPCC, 2018).

However, changes in temperature under global warming are associated with latitude rather than regional climate characteristics (Dong et al., 2018). TX90P (TN90P) change patterns derived from MME are related to the area-averaged latitude in each climate zone (Figure 5b, d). The negative relationship between TX90P (TN90P) and area-averaged latitude indicates that a

280 significant increases in the extreme hottest temperatures (exceeding 90th percentile) more frequently occur in low-latitude regions. Among the 12 climate zones, the largest changes are observed in tropical climate zones (Af, Am, and Aw) in both TX and TN. These results imply that tropical climate regions with lowest interannual temperature variability, are very sensitive to warmer temperatures as demonstrated in IPCC (2018). This robust behavior is more prevalent in TN90P because its' sensitivity

to global temperature increases is higher than TX90P. Overall, global warming above PI levels affects strong changes in the

285   distributions of maximum and minimum temperature (e.g., TX, TN) at daily time scale and the directions of the projected changes trend toward an enhancement at high-percentile temperatures compared to the REF regardless of the climatic characteristics, which may in turn lead to increased risks of heatwaves as well as temperature-based seasonal cycle changes.

3.3 Future projections of precipitation extremes under 1.5 and 2.0 °C of warming

Anthropogenic forcings have attributed to the intensification of regional precipitation extremes (e.g., O'Gorman, 2015; Weber

290   et al., 2018; Guo et al., 2016). We examine future change of precipitation from MME of the five GCMs under two global warming scenarios (e.g., 1.5 and 2.0 °C). The regions with the 100 % and 80 % of intermodel agreement on change signal are identified for the analysis in section 3.3 and 3.4 to provide a level of the robustness of future change patterns.

Figure 6 displays the relative changes in extreme precipitation (P95, P99) on its amount, frequency and intensity under 1.5 and 2.0 °C condition in comparison to the REF, and global warming tends to intensify the amounts, frequency and intensity of

295   extreme precipitation over Asia. Overall, significant increases in both P95 and P99 under 1.5 and 2.0 °C conditions, are shown in most of the climate zones. In particular, increasing change signals at both P95 and P99 at 2.0 °C condition are stronger than those at 1.5 °C condition (Figure 6a, b, c). In most regions, changes at P99 are larger and more significant with regard to the total amount, frequency as well as intensity than changes at P95. The largest difference between P95 and P99 is the intensity change. While the magnitude of change is smallest in terms of the intensities of both P95 and P99 rather than in total amount

300   and frequency, the robustness is largest in terms of intensity change.

Figure 7a presents a spatial distribution of change in annual maximum precipitation (PX1D) under 1.5 and 2.0 °C in comparison with that under REF. The consistent pattern are shown in an increase in PX1D (except for several grids that showed reduced changes in both the 1.5 and 2.0 °C conditions). As the globe warms, the intensity of extreme precipitation consistently increases in most regions of Asia (93.1 % of whole domain at 1.5 °C; 96.8 % of whole domain at 2.0 °C). As shown in this result, the

305   increasing signals over the study area become more apparent and robust with 4 out of 5 under 2.0 °C than 1.5 °C condition. This result implies an intensification of extreme precipitation. Most of the grids where increasing signal is shown in PX1D over Asia, are likely to increase by 2, 3, and 5 consecutive days of maximum precipitation (PX2D, PX3D, and PX5D) under both 1.5 and 2.0 °C of warming in comparison to the REF. The spatial distribution of change patterns in PX2D, PX3D, and PX5D is similar to that of PX1D under both 1.5 and 2.0 °C scenarios (Figure 7b). The pattern correlation coefficients (PCC)

310   among PX1D and PX2D, PX3D, and PX5D are 0.89, 0.83, and 0.73, respectively. And, the PCC differences between 1.5 and 2.0 °C are not significant in all cases. As shown this PCC results, the change pattern of PX1D is highly correlated with that of others (e.g., PX2D, PX3D, and PX5D) in terms of spatial distribution. These results describe the intensification of extremes precipitation with similar spatial behavior under warmer climate conditions.

Figure 8 presents the area-averaged changes in PANN and PX1D compared to REF under 1.5 and 2.0 °C conditions. Changes

315   in PX1D are greater than the changes in PANN in most climate zones except Bs and Bw (Figure 7a). PANN increases under global warming compared with REF, with increases from 1.4 % to 8.6 % for 1.5 °C condition and from 3.5 % to 10.6 % for 2.0 °C condition. Meanwhile, PX1D is projected to significantly increase from 4.3 % to 9.8 % under 1.5 °C condition and from 5.8 % to 15.8 % under 2.0 °C condition. The 2.0 °C warming results in higher precipitation in terms of both PANN and PX1D than 1.5 °C. Under warmer climate environment, PX1D over all climate zones is expected to increase with a high level of

320   robustness compared to PANN. Global warming will lead to adverse influences on the risk of flooding over Asia region due to an increase of precipitation events with high-intensity, especially in 2.0 °C warming.

3.4 Future projections of runoff extremes under 1.5 and 2.0 °C of warming

In this section, we examine the future change in runoff based on the VIC simulations, which are fed with the individual five GCMs. Figure 9 indicates the spatial distribution of changes in extreme high and low runoff over Asia based on the 1.5 and

325   2.0 ℃ warming scenarios. The consistent patterns with 4 out of 5 are shown in an increase of annual maximum runoff (MDF) across most regions (except for several grids under 2.0 ℃ condition). The result implies intensified extremely high runoff, which in turn may increase the risk of flooding. Meanwhile, the low runoff (7-days and 30-days of minimum runoff; DWF07 and DWF30) are different change signals according to the region under 1.5 and 2.0 ℃ conditions over Asia. As warming intensifies, increases in both DWF07 and DWF30 become more dominant than decreases in both DWF07 and DWF30 over

330   Asia. However, as highlighted regions with green and yellow in Figure 9, some regions of the Cf and Bw zones, which are shown with consistent decreasing patterns for both 1.5 and 2.0 ℃ conditions. As the temperature increases, the regions are likely to be susceptible to DWF07 and DWF30. Because the precipitation patterns are transferred to runoff features (Kim et al., 2019), the changes in runoff patterns in terms of the spatial distribution and an increasing (or decreasing) signal show a large similarity to precipitation patterns, especially in change patterns between PX1D and MDF.

335   Figure 10 represents the area-averaged changes of annual mean runoff and high runoff (i.e., MDF) compared to REF under 1.5 and 2.0 ℃ conditions. Changes of annual mean runoff (hereafter referred to as RANN) increase in all climate zones under global warming compared with REF. Changes in MDF also increase in most of the climate zones except the Ds zone, which shows a large variation among the five GCMs. The magnitude of MDF over Asia is projected to be greater than REF, especially under 2.0 ℃ condition compared to 1.5 ℃ condition in the greater part of the climate zones (e.g., all A, C, E zone, Bw, and

340   Ds zone). A 2.0 ℃ of global warming causes the a sharp increase in runoff in terms of both RANN and MDF than a 1.5 ℃, which implies the intensification of runoff as the global warming enhanced. As with changes in precipitation, an increase in MDF over all climate zones shows the considerable degree of robustness compared to RANN at 1.5 and 2.0 ℃ warming climate environments. Warming over Asia will aggravate the management of water resources due to challenging situation, such as an increase in MDF and a large spatial disparity of changes in DWF07 and DWF30.

345   4 Discussion and conclusions

As suggested by the IPCC, it is likely that anthropogenic influences have affected the global climate system, and such effects increase the likelihood of more intense extreme climate events (e.g., heatwaves, precipitation, flooding, and droughts) worldwide (IPCC, 2013; 2018). An extreme climate event is a phenomenon that occur at a level above (or below) a threshold defined by a normal range within a given region for each variable. And, it is closely related to the climate features of certain

350   region. Therefore, to minimize damage from climate disasters under global temperature increases of 1.5 and 2.0 ℃ above PI levels, it is important to analyze regional changes in both long-term climate patterns and climate extremes (Kharin et al., 2018; Dong et al., 2018).

Table 5 presents the relative changes (%) in average hydroclimates and extreme hydroclimates under further 0.5 ℃ increase from the difference between the 1.5 and 2.0 ℃ of global mean temperature in each climate zone. In general, all the changes in

355   extreme hydroclimates except for runoff extremes (MDF, DWF07, and DWF30) exhibit similar change patterns in each climate zone under an extra 0.5 ℃ of warming. However, the influence of an extra increase of 0.5 ℃ on extreme hydroclimates shows the diverse change patterns and magnitudes according to regions and types of extreme climate indices. Changes in temperature extremes represent significant change patterns with a high degree of robustness over all climate zones. As the globe warms, changes in warm extreme indices (e.g., SU, TR, TX90P, and TN90P) indicate an increasing trend over most climate zones,

360   except for SU and TR in the Af and ET zones. On the other hand, the cold extreme indices (e.g., FD, ID, TX10P, and TN10P) have a distinct tendency to increase across Asia. Significant increases in extreme warm indices are shown in arid climates (BS and BW) and cold climates (Ds, Dw, and Df), whereas a large decrease in warm temperate climates (Cs, Cw and Cf) is projected. Next, high-precipitation changes (e.g., P95, P99, PX1D, PX2D, PX3D, and PX5D) exhibit large and significant increasing patterns compared to PANN according to an extra 0.5 ℃ of warming. The change in MDF shows a similar result to PX1D

365   because the change pattern of precipitation has an influence on that of runoff. The results represent an increase in the risk of

runoff and flooding in most climate zones over Asia. Relatively, the change in the Cs and Ds zones with dry summer features shows somewhat greater variability in terms of both averages and extremes in precipitation (and runoff) under an extra 0.5 ℃ warming climate environment. In general, in comparison with MDF, change patterns of low runoff (DWF07 and DWF30) show a relatively less robust pattern, especially in terms of lower magnitude of change amount or in decreasing change signal

370   (e.g., MacDonald et al., 2018). Even though, the future projections of low runoff contain levels of uncertainty due to variation among the individual GCMs, Cf and Bw zones are likely to face challenges to cope with low runoff under global warming (Figure 9).

Overall, D and E zone are highly susceptible to an extra 0.5 ℃ of warming. This regions show significant changes in temperature extremes, high-precipitation extremes and high-runoff extremes, which is suggested in Table 5. The area-average

375   cold extremes in this region are expected to decrease by -4.0 % (FD) and -6.8 % (ID), while warm extremes are projected to largely increase by 57.2 % (SU) and 80.8 % (TR). The projected changes in high-precipitation extremes are indicated to be approximately 3.3~3.6 % increases for PX1D, PX2D, PX3D, and PX5D and approximately 10.5 % and 18.7 % increases for P95 and P99, respectively. Subsequently, a high-runoff extreme is expected to increase by 3.4 %, which is likely to result in a more intensified flooding risk. In contrast, changes in low extreme runoff, such as those in DWF07 and DWF30, show

380   nonsignificant change signals in this the regions, which results from small changes under 0.5 ℃ global warming and a substantial uncertainty in GCM projections, and this finding agrees with the previous results (e.g., Chen et al., 2017; Donnelly et al., 2017; Marx et al., 2018).

We focus upon the changes in extreme hydroclimates across diverse climate characteristics over the Asia in response to 1.5 and 2.0 ℃ of warming scenarios under stabilization emission forcings (RCP4.5) above the PI level. The five GCMs

385   participating in CMIP5 are selected considering their performance of the historical simulations. The central year and 30-year period reaching 1.5 and 2.0 ℃ warming targets are identified based on the individual GCMs. Five GCMs after removing systematic biases used as a meteorological forcing for distributed hydrological model (VIC) and the simulated surface runoff is then converted to area-averaged runoff according to climate zones. Future changes in various extreme indices (e.g., temperature, precipitation, runoff-related indices) are calculated from the relative concept existed in the difference between

390   the individual warming conditions (1.5 and 2.0 ℃) and REF. Our focus is to estimate and compare the change patterns of extreme temperature, precipitation, and runoff among the various climate zones under 1.5 and 2.0 ℃ global warming.

In all climate zones, an extra 0.5 ℃ of global warming condition has a considerable influence on changes in extreme hydroclimates. Changes in temperature, which show the strongest robustness over Asia, with 5 out 5, are projected toward a greater increase in high-percentile maximum and minimum temperatures. Although there is a great uncertainty in the

395   precipitation and runoff projections, the results of high-precipitation and high-runoff extremes show increasing patterns with a high level of robustness. This result support the concept that global warming leads to an intensified hydrological response, such as an increase in high-precipitation extremes (e.g., Trenberth, 1999; Giorgi et al., 2014; Im et al., 2017; Kim et al., 2019). Subsequently, consistent with the change pattern of precipitation, high-runoff extremes under warmer condition are likely to increase the risks of water-related disasters in most climate zones of Asia. Our findings are generally consistent with previous

400   studies that have suggested likely increased high-runoff extremes under warmer climates conditions above REF (e.g., MacDonald et al., 2018; Jacob et al., 2018; Paltan et al., 2018; Kim et al., 2019). Although the behaviors are taken from a limited number of GCMs, our findings derived from the CMIP5 multimodel mean show accelerated extremes compared to long-term mean. Since the hydroclimatic sensitivity differ based on regional climate characteristics, understanding change behavior of hydroclimatic extremes is required in terms of regional scale.

405 **Code and data availability**

VIC model code is publicly available at https://vic.readthedocs.io/en/master/SourceCode/Code/. USGS DEM data (i.e., GTOPO30) is available at https://earthexplorer.usgs.gov/. Meteorological forcing data used in this study can be found in the APHRODITE (http://www.chikyu.ac.jp/precip/english/products.html) and in Global datasets of VIC model (https://vic.readthedocs.io/en/master/Datasets/Datasets/), and ECMWF (CERA-20C;

410 https://www.ecmwf.int/en/forecasts/datasets/reanalysis-datasets/cera-20c). More information of the data could be obtained by emailing the correspondence author or the first author.

Author contributions

JBK designed and carried out the study. DHB supervised the project. All the authors contributed to the writing and the interpretation of the results.

415 **Competing interests**

The authors declare that they have no conflict of interest.

Acknowledgments

420 **References**

Adam, J.C. and Lettenmaier, D.P.: Adjustment of global gridded precipitation for systematic bias, Journal of Geophysical Research, 108, 1-14, https://doi:10.1029/2002JD002499, 2003.

Adam, J.C., Clark, E.A., Lettenmaier, D.P. and Wood, E.F.: Correction of Global Precipitation Products for Orographic Effects, Journal of Climate, 19, 15-38, https://doi: 10.1175/JCLI3604.1, 2006.

425 Bae, D.H., Jung, I.W. and Lettenmaier, D.P.: Hydrologic Uncertainties in Climate Change from IPCC AR4 GCM Simulation of the Chungju Basin, Korea, Journal of Hydrology, 401, 90-105, 2011.

Bae, D.-H., Rahman, M., Koike, T. and Ahmad, B.: Climate change impact assessment on the Asia-Pacific water resources under AWCI/GEOSS, Final Report of the APN ARCP Project: ARCP2011-05CMY-Bae, Asia-Pacific Network for Global Change Research, 2013

430 Bae, D.H, Koike, T., Awan, J.A., Lee, M.H. and Son, K.H.: Climate Change Impact Assessment on Water Resources and Susceptible Zones Identification in the Asian Monsoon Region, Water Resources Management, 29, 5377-5393, 2015.

Beck, H.E., van Dijk, A.I.J.M., deRoo, A., Miralles, D.G., McVicar, T.R., Schellekens, J. and Bruijnzeel, L.A.: Global-scale regionalization of hydrologic model parameters. Water Resources Research, 52, 3599-3622. https://doi.org/10.1002/2015WR018247, 2016.

435 Bhowmick, M., Sahany, S. and Mishra, S.K.: Projected precipitation changes over the south Asian region for every 0.5℃ increase in global warming, Environmental Research Letters, 14, 054005, 2019.

Chen, J., Gao, C., Zeng, X., Xiong, M., Wang, Y., Jing, C., Krysanova, V., Huang, J., Zhao, Na. and Su, B.: Assessing changes of river discharge under global warming of 1.5℃ and 2℃ in the upper reaches of the Yangtze River Basin: Approach by using multiple-GCMs and hydrological models, Quaternary International, 453, 2017.

440 Chen, S., Zhi-Hong, J., Wei-Lin, C. and LI, L.: Changes in temperature extremes over China under 1.5℃ and 2℃ global warming targets, Advances in Climate Change Research, 9, 120-129, 2018.

Chevuturi, A., Klingaman, N P., Turner, A.G. and Hannah, S.: Projected Changes in the Asian-Australian Monsoon Region in 1.5℃ and 2.0℃ Global-Warming Scenarios, Earth's Future, 6, 339-358, 2018.

Diedhiou, A., Bichet, A., Wartenburge, R., Seneviratne, S.I., Rowell, D.P., Sylla, M.B., Diallo, I., Todzo, S., Touré, N.E.,
445 Camara, M., Ngatchah, B.N., Kane, N.A., Tall, L. and Affholder, F.: Changes in climate extremes over West and Central Africa at 1.5 °C and 2 °C global warming, Environmental Research Letters, 13, 065020, https://doi.org/10.1088/1748-9326/aac3e5, 2018.

Donnelly, C., Greuell, W., Andersson, J., Gerten, D., Pisacane, G., Roudier P. and Ludwig, F.: Impacts of climate change on European hydrology at 1.5, 2 and 3 degrees mean global warming above preindustrial level, Climatic Change, 143, 13-26,
450 2017.

Dong, S., Aguilar, E., Zhang, X., Peterson, T.C., Song, L. and Zhang, Y.: (2018) Observed changes in temperature extremes over Asia and their attribution, Climate Dynamics, 51, 339-353.

Dosio, A. and Fischer, E.M.: Will half a degree make a difference? Robust projections of indices of mean and extreme climate in Europe under 1.5 °C, 2 °C, and 3 °C global warming, Geophysical Research Letters, 45, 935-944, 2018.

455 FAO: World Reference Base for Soil Resources. World Soil Resources Reports 84, Rome: FAO (Food and Agriculture Organization of the United Nations), 1998.

Fernandez, J.P.R., Franchito, S.H., Rao, V.B. and Llopart, M.: Changes in Koppen–Trewartha climate classification over South America from RegCM4 projections, Atmospheric Science Letters, 18, 427-434, 2017.

Ge, F., Zhu, S., Peng, T., Zhao, Y., Sielmann, F., Fraedrich, K., Zhi, X., Liu, X., Tang, W. and Ji, L.: Risks of precipitation
460 extremes over Southeast Asia: does 1.5 °C or 2 °C global warming make a difference? Environmental Research Letters, 14, 044015, 2019.

Giorgi, F., Coppola, E. and Raffaele, F.: A consistent picture of the hydroclimatic response to global warming from multiple indices: Models and observations, Journal of Geophysical Research: Atmospheres, 119, 11695-11708, https://doi:10.1002/2014JD022238, 2014.

465 Guo, X., Huang, J., Luo, Y., Zhao, Z. and Xu, Y.: Projection of precipitation extremes for eight global warming targets by 17 CMIP5 models, Natural Hazards, 84, 2299-2319, 2016.

Hansen, M.C., Defries, R.S., Townshend, J.R.G. and Sohlberg, R. Global land cover classification at 1 km spatial resolution using a classification tree approach, International Journal of Remote Sensing, 21, 1331-1364, https://doi.org/10.1080/014311600210209, 2000.

470 Harrington, L.J. and Otto, F.E.L.: Changing population dynamics and uneven temperature emergence combine to exacerbate regional exposure to heat extremes under 1.5 °C and 2 °C of warming, Environmental Research Letters, 13, 034011, 2018.

Im, E.S., Choi, Y.W. and Ahn, J.B.: Robust intensification of hydroclimatic intensity over East Asia from multi-model ensemble regional projections, Theoretical and Applied Climatology, 129, 1241-1254, https://doi.org/10.1007/s00704-016-1846-2, 2017.

475 IPCC: Climate Change 2013: The Physical Science Basis. Contribution of Working Group I to the Fifth Assessment Report of the Intergovernmental Panel on Climate Change, Cambridge and New York, NY: Cambridge University Press, 2013.

IPCC: Global warming of 1.5℃. An IPCC Special Report on the impacts of global warming of 1.5℃ above pre-industrial levels and related global greenhouse gas emission pathways, in the context of strengthening the global response to the threat of climate change, sustainable development, and efforts to eradicate poverty [V. Masson-Delmotte, P. Zhai, H. O.
480 Pörtner, D. Roberts, J. Skea, P.R. Shukla, A. Pirani, W. Moufouma-Okia, C. Péan, R. Pidcock, S. Connors, J. B. R. Matthews, Y. Chen, X. Zhou, M. I. Gomis, E. Lonnoy, T. Maycock, M. Tignor, T. Waterfield (eds.)]. In Press, 2018.

Jacob, D., Kotova, L., Teichmann, C., Sobolowski, S.P., Vautard, R., Donnelly, C., Koutroulis, A.G., Grillakis, M.G., Tsanis, I.K., Damm, A., Sakalli, A. and van Vliet, M.T.H.: Climate Impacts in Europe Under +1.5∘ C Global Warming, Earth's Future, 6, https://doi .org/10.1002/2017EF000710, 2018.

485   James, R., Washington, R., Schleussner, C.-F., Rogelj, J. and Conway, D.: Characterizing half-a-degree difference: a review of methods for identifying regional climate responses to global warming targets, WIREs Climate Change, 8, https://doi.org/10.1002/wcc.457, 2017.

Jiao, Y. and Yuan, X.: More severe hydrological drought events emerge at different warming levels over the Wudinghe watershed in northern China, Hydrology Earth System Science, 23, 621-635, 2019.

490   Jung, I.W., Bae, D.H. and Lee, B.J.: Possible change in Korean streamflow seasonality based on multi-model climate projections, Hydrological Processes, 27, 1033-1045, 2013.

Kharin V.V., Flato, G.M., Zhang, X., Gillett, N.P., Zwiers, F. and Anderson, K.J. Risks from Climate Extremes Change Differently from 1.5°C to 2.0°C Depending on Rarity, Earth's Future, 6, 704-715, 2018.

Kim, J.-B., Im, E.-S. and Bae, D.-H.: Intensified hydroclimatic regime in Korean basins under 1.5 and 2℃ global warming,
495   International Journal of Climatology, https://doi.org/ 10.1002/joc.6311, 2019.

King, A.D. and Karoly, D.: Climate extremes in Europe at 1.5 and 2 degrees of global warming, Environmental Research Letter, 12, 114031, https://doi.org/10.1088/1748-9326/aa8e2c, 2017.

Köppen, W.: Das geographische System der Klimate, In: Köppen W, Geiger R (eds) Handbuch der Klimato logie, Gebrüder Borntraeger, Berlin, 1936.

500   Laloyaux, P., de Boisseson, E., Balmaseda, M., Bidlot, J.R., Broennimann, S., Buizza, R., Dalhgren, P., Dee, D., Haimberger, L., Hersbach, H., Kosaka, Y., Martin, M., Poli, P., Rayner, N., Rustemeier, E. and Schepers, D.: CERA-20C: A coupled reanalysis of the twentieth century, Journal of Advances in Modeling Earth Systems, 10, 1172-1195, https://doi.org/10.1029/2018MS001273, 2018.

Lee, M.-H. and Bae, D.-H.: Climate change impact assessment on green and blue water over Asian monsoon region, Water
505   Resources Management, 29, 2407-2427, 2015.

Li, D., Zhou, T., Zou, L., Zhang, W. and Zhang, L.: Extreme High-Temperature Events Over East Asia in 1.5℃ and 2℃ Warmer Futures: Analysis of NCAR CESM Low-Warming Experiments, Geophysical Research Letters, 45, 1541-1550, https://doi.org/10.1002/2017GL076753, 2018.

Liang, X., Lettenmaier, D.P., Wood, E.F. and Burges, S.J.: A simple hydrologically based model of land surface water and
510   energy fluxes for general circulation models, Journal of Geophysical Research, 99, 14415-14428, 1994.

Liang, X., Wood, E.F. and Lettenmaier, D.P.: Surface soil moisture parameterization of the VIC-2L model: Evaluation and modifications, Global and Planetary Change, 13, 195-206, 1996.

Maurer, E.P. and Pierce, D.W.: Bias correction can modify climate model simulated precipitation changes without adverse effect on the ensemble mean, Hydrology and Earth System Sciences, 18, 915-925, https://doi.org/10.5194/hess-18-915-
515   2014, 2014.

Marx, A., Kumar, R., Thober, S., Rakovec, O., Wanders, N., Zink, M., Wood, E.F., Pan, M., Sheffield, J. and Samaniego, L.: Climate change alters low flows in Europe under global warming of 1.5, 2, and 3 ℃, Hydrology and Earth System Sciences, 22, 1017-1032, 2018.

MacDonald, M.K., Stadnyk, T.A., Déry, S.J., Braun, M., Gustafsson, D., Isberg, K. and Arheimer, B.: Impacts of 1.5 and
520   2.0℃ warming on pan-Arctic river discharge into the Hudson Bay Complex through 2070, Geophysical Research Letters, 45, 7561-7570, 2018.

Nandintsetseg, B., Greene, J.C. and Goulden, C.E.: Trends in extreme daily precipitation and temperature near Lake Hovsgol, Mongolia, International Journal of Climatology, 27, 341-347, 2007.

525   Nkemelang, T., New, M. and Zaroug, M.: Temperature and precipitation extremes under current, 1.5 ℃ and 2.0 ℃ global warming above pre-industrial levels over Botswana, and implications for climate change vulnerability. Environmental Research Letter, 13, 065016, https://doi.org/10.1088/1748-9326/aac2f8, 2018.

Nyunt, C.T., Yamamoto, H., Yamamoto, A. and Koike, T.: Application of biascorrection and downscaling method to Kalu Ganga basin in Sri Lanka, Annual Journal of Hydraulics Engineering-JSCE, 56, 115-120, 2012.

O'Gorman, P.A.: Precipitation Extremes Under Climate Change, Current Climate Change Reports, 1, 49-59, 2015.

530   Paltan, H., Allen, M., Haustein, K., Fuldauer, L. and Dadson, L.: Global implications of 1.5℃ and 2℃ warmer worlds on extreme river flows, Environmental Research Letter, 13, 094003, https://doi.org/10.1088/1748-9326/aad985, 2018.

Parajka, J., Merz, R. and Bloschl, G.: A comparison of regionalisation methods for catchment model parameters, Hydrology and Earth System Sciences, 9, 157-171, 2005.

Parajka, J., Viglione, A., Rogger, M., Salinas, J.L., Sivapalan, M. and Bloschl, G.: Comparative assessment of predictions in
535   ungauged basins: Part 1: Runoff-hydrograph studies, Hydrology and Earth System Sciences, 17, 1783-1795, 2013.

Sheffield, J., Andreadis, K., Wood, E. and Lettenmaier, D.: Global and continental drought in the second half of the twentieth century: severity-area-duration analysis and temporal variability of large-scale events, Journal of Climate, 22, 1962-1981, 2009.

Sui, Y., Lang, X. and Jiang, D.: Projected signals in climate extremes over China associated with a 2 ℃ global warming under
540   two RCP scenarios, International Journal of Climatology, 38, e678–e697, https://doi.org/10.1002/joc.5399, 2018.

Sylla, M.B., Faye, A., Giorgi, F., Diedhiou, A. and Kunstmann, H.: Projected heat stress under 1.5 ℃ and 2 ℃ global warming scenarios creates unprecedented discomfort for humans in West Africa, Earth's Future, 6, 1029-1044. https://doi.org/10.1029/2018EF000873, 2018.

Taylor, K.E., Stouffer, R.J. and Meehl, G.A.: An overview of CMIP5 and the experiment design, Bulletin of the American
545   Meteorological Society, 93, 485-498, 2012.

Thomson, A.M., Calvin, K.V., Smith, S.J., Kyle, G.P., Vloke, A., Patel, P., Delgado-Arias, S., Bond-Lamberty, B., Wise, M.A., Clarke, L.E. and Edmond, J.A.: RCP4.5: a pathway for stabilization of radiative forcing by 2100, Climatic Change, 109, 2011.

Trenberth, K.E.: Conceptual framework for changes of extremes of the hydrological cycle with climate change, Climatic
550   Change, 42, 327-339, 1999.

Trenberth, K.E.: Changes in precipitation with climate change, Climatic Research, 47, 123-138, 2011.

UNFCCC: Report of the Conference of the Parties on its twenty-first session, held in Paris from 30 November to 13 December 2015. Part two: Action taken by the Conference of the Parties at its twenty-first session. United Nations. FCCC/CP/2015/10/Add.1, http://unfccc.int/resource/docs/2015/cop21/eng/10a01.pdf, 2015.

555   Van Vuuren, D.P., Edmonds, J., Kainuma, M., Riahi, K., Thomson, A., Hibbard, K., Hurtt, G.C., Kram, T., Krey, V., Lamarque, J.-F., Masui, T., Meinshausen, M., Nakicenovic, N., Smith, S.J. and Rose, S.K.: The representative concentration pathways: an overview, Climatic Change, 109, 2011.

Yatagai, A., Kamiguchi, K., Arakawa, O., Hamada, A., Yasutomi, N. and Kitoh, A.: APHRODITE: Constracting a Long-Term Daily Gridded Precipitation Dataset for Asia Based on a Dense Network of Rain Gauges, Bulletin of the American
560   Meteorological Society, 93, 1401-1415. https://doi:10.1175/BAMS-D-11-00122.1, 2012.

Wang, X., Jiang, D. and Lang, X.: Extreme temperature and precipitation changes associated with four degree of global warming above pre-industrial levels, International Journal of Climatology, 39, 1822-1838. https://doi.org/10.1002/joc.5956, 2019.

Weber, T., Haensler, A., Rechid, D., Pfeifer, S., Eggert, B. and Jacob, D.: Analyzing Regional Climate Change in Africa in a
565   1.5, 2, and 3℃ Global Warming World, Earth's Future, 6, 643-655, 2018.

Wen, S., Wang, A., Tao, H., Malik, K., Huang, J., Zhai, J., Jing, C., Rasul, G. and Su, B.: Population exposed to drought under the 1.5 ℃ and 2.0 ℃ warming in the Indus River Basin, Atmospheric Research, 218, 296-305, 2019.

Zhang, Y., You, Q., Mao, G., Chen, C. and Ye, Z.: Short-term concurrent drought and heatwave frequency with 1.5 and 2.0 ℃ global warming in humid subtropical basins: a case study in the Gan River Basin, China, Climate Dynamics, 52, 4621-
570   4641, 2019.

Zhou, M., Zhou, G., Lv, X., Zhou, L. and Ji, Y.: Global warming from 1.5 to 2 ℃ will lead to increase in precipitation intensity in China. International Journal of Climatology, https://doi.org/10.1002/joc.5956, 2018.
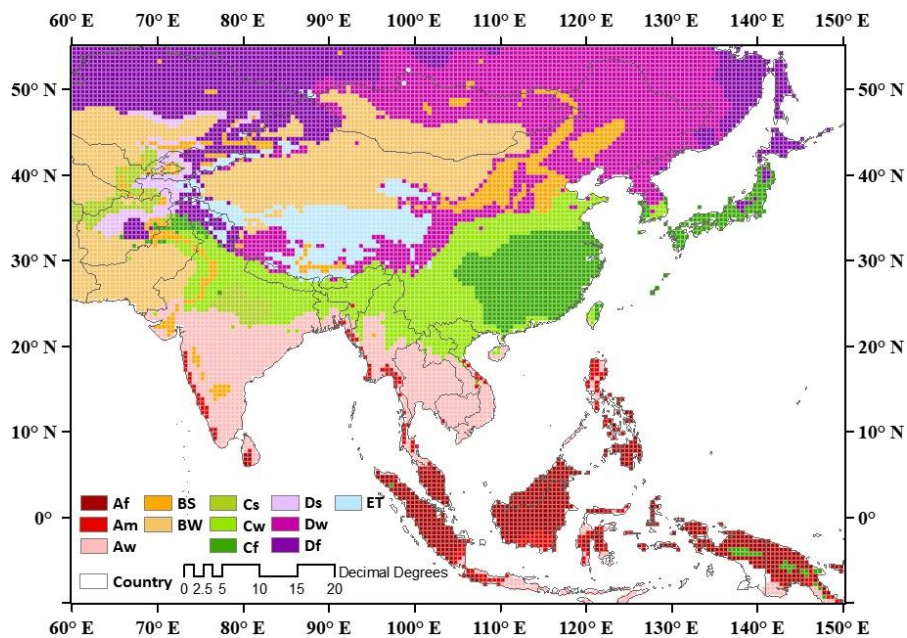
Figure 1: Study domain range, climate zone classifications and 10,977 grid points of the VIC model used for analysis in this study. The 12 grid colors indicate the climate zones that are classified based on the Köppen climate zone method.
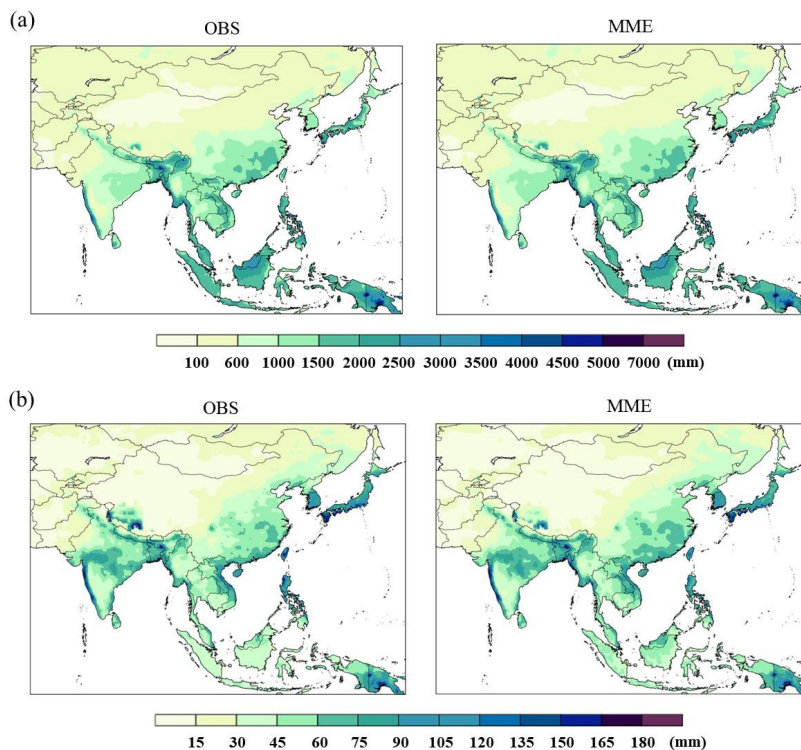
Figure 2: Spatial distribution of (a) annual mean precipitation and (b) annual maximum precipitation (PX1D) for the historical period (1976-2005) in the Asia monsoon region derived from observations and the MME of bias-corrected outputs from the five GCMs.

580
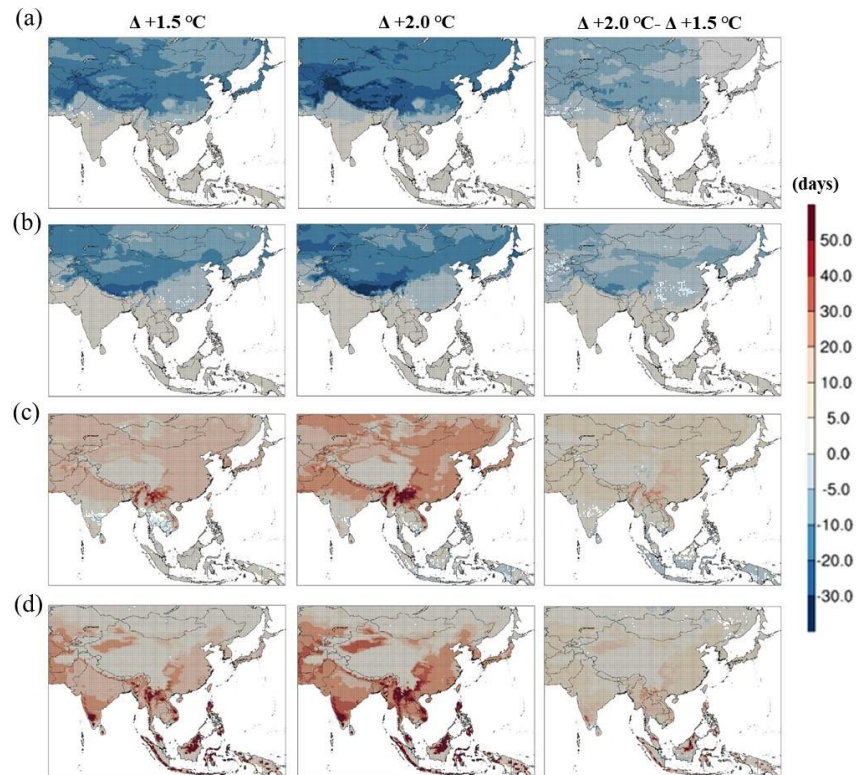
Figure 3: Spatial distribution of Multimodel ensemble (MME) for extreme climate indices (FD, ID, SU and TR) over the study domain. Relative changes in (a) FD, (b) ID, (c) Summer days (SU), and (d) Tropical nights (TR) under 1.5 °C and 2.0 °C global warming are compared to those of the REF.

585
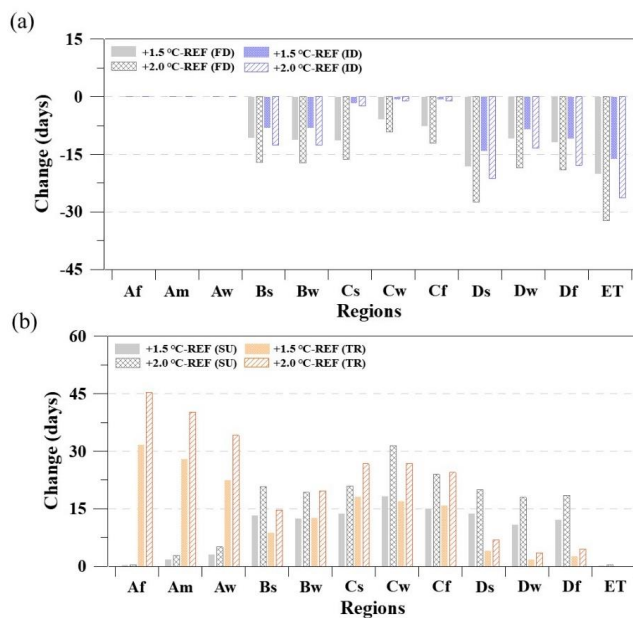
Figure 4: Changes in extreme temperature indices (a) related to the coldest days (FD and ID) and (b) hottest days (SU and TR)
590   **derived from MME for 12 climate zones.**

Hydrology and
Earth System
Sciences
Open Access
Discussions
EGU
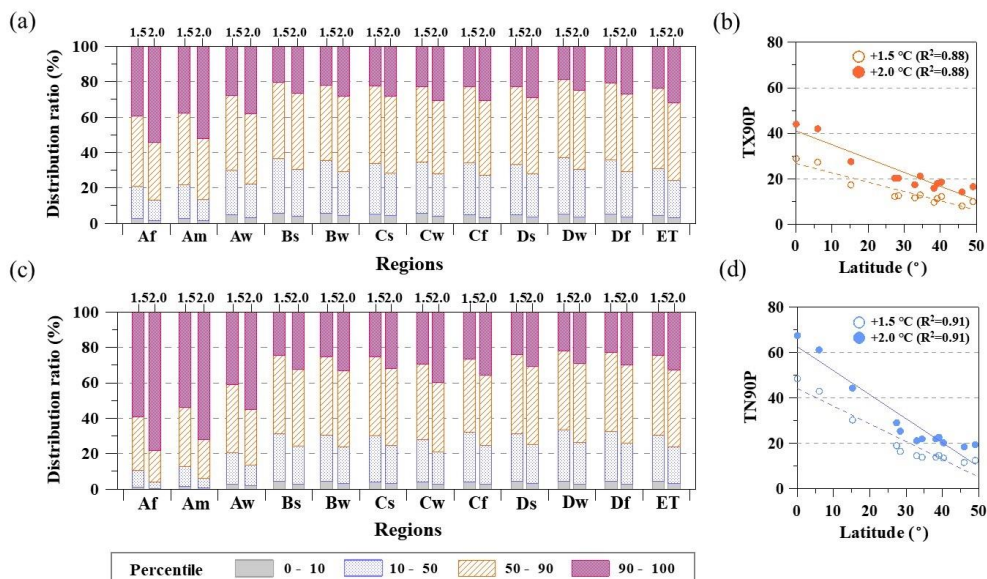
Figure 5: Relative changes in (a, c) maximum temperature (TX) and minimum temperature (TN) according to four percentile ranges under 1.5 and 2.0 °C of global warming compared to the REF. (b, d) The relationship between the average latitude of each climate zone and relative changes in the 90th percentile of maximum temperature (TX) and minimum temperature (TN) under global warming.

Hydrology and
Earth System
Sciences
Open Access
Discussions
EGU
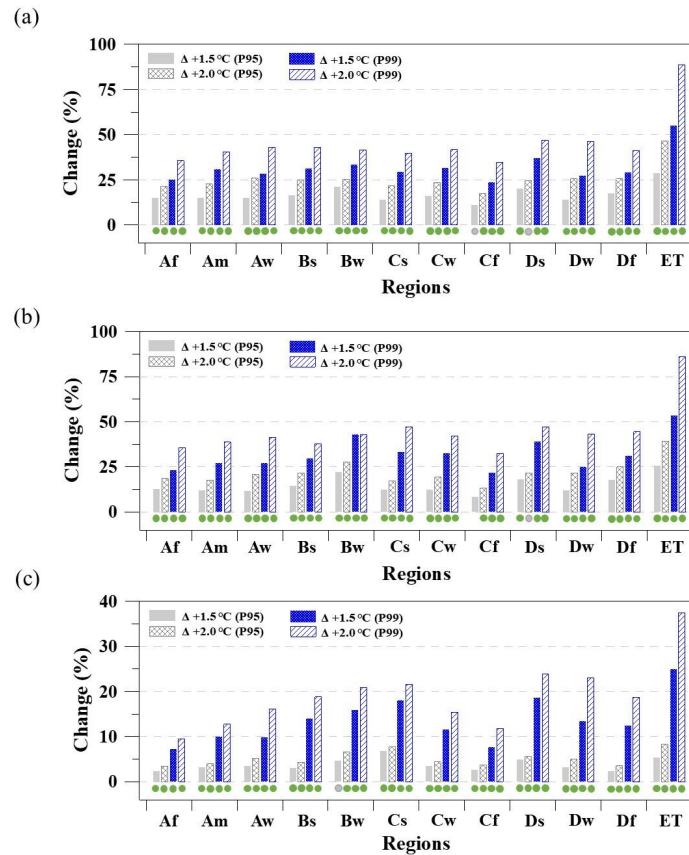
Figure 6: Relative changes in (a) total amount, (b) frequency and (c) intensity of extreme precipitation indices (R95 and R99) for 12 climate zones derived from the multimodel ensemble (MME) of five GCMs under 1.5 °C and 2.0 °C of global warming compared to the REF. Green circles (gray circles) denote over 100 % (80 %) intermodel agreement.

Hydrology and
Earth System
Sciences
Open Access
Discussions
EGU
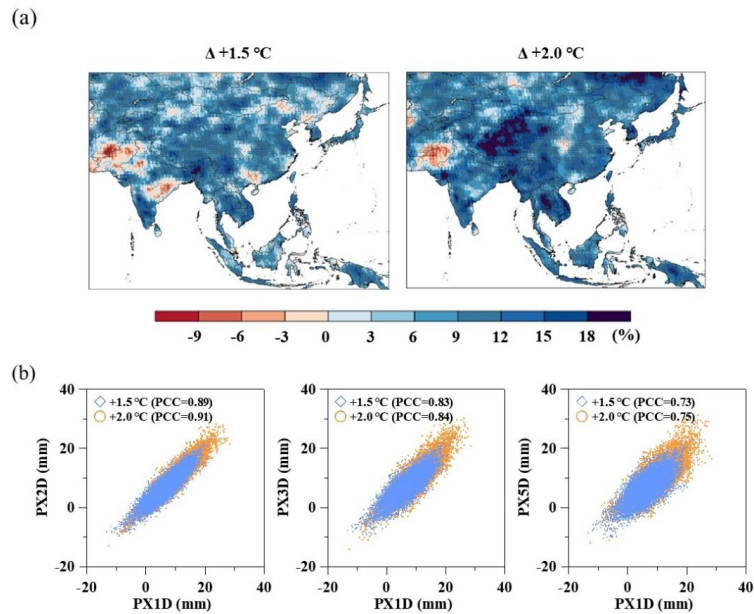
Figure 7: (a) Relative changes in the annual maximum precipitation (PX1D) derived from the MME of five GCMs under 1.5 °C and 2.0 °C of global warming compared to the REF. (b) Comparison of relative changes among maximum precipitation over 2, 3 and 5 consecutive days (PX2D, PX3D, and PX5D, respectively) with PX1D derived from MME over the Asia monsoon region.

Hydrology and
Earth System
Sciences
Open Access

Discussions

EGU
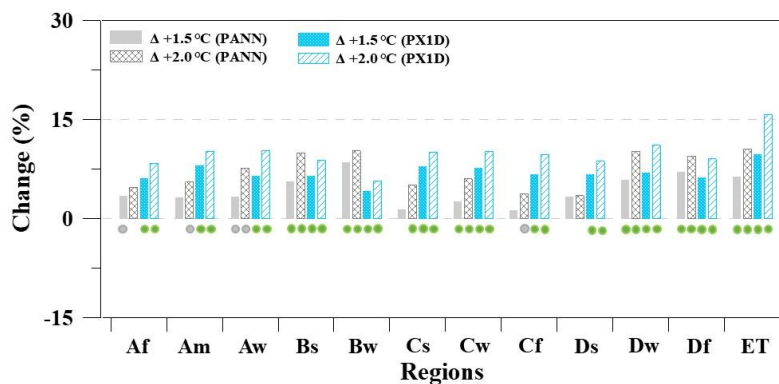
610

Figure 8: Relative changes in annual mean precipitation and annual maximum precipitation (PX1D) for 12 climate zones derived from the MME of five GCMs under 1.5 °C and 2.0 °C of global warming compared to the REF. Green circles (gray circles) denote over 100 % (80 %) intermodel agreement.

Hydrology and
Earth System
Sciences
Discussions
Open Access
EGU
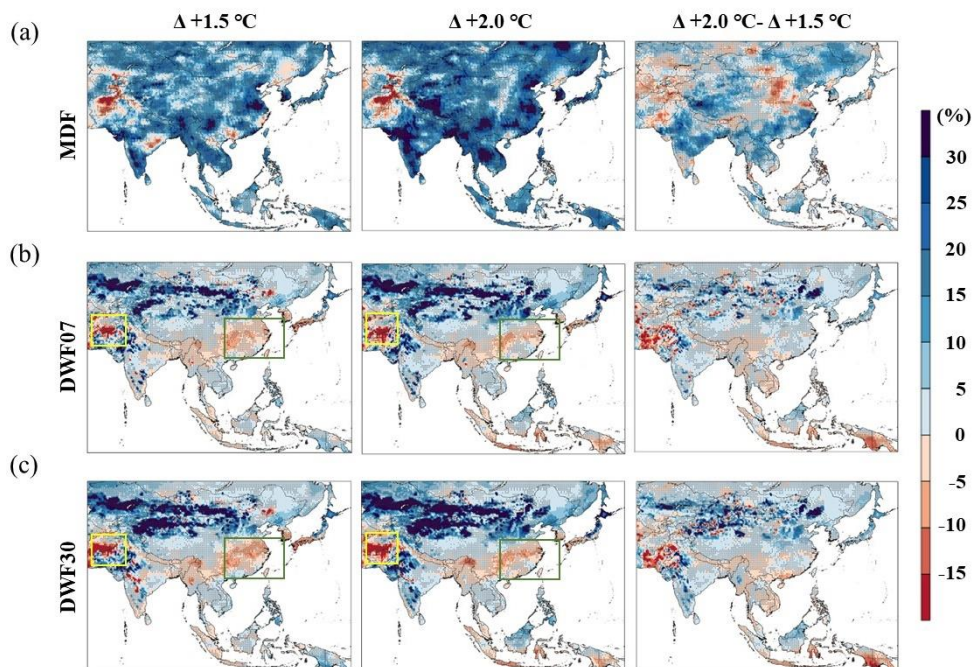
Figure 9: Spatial distribution of MME for extreme climate indices (MDF, DWF07, and DWF30) over the study domain. Relative changes in (a) annual maximum runoff (MDF), (b) consecutive 7-day minimum runoff (DWF07), and (c) consecutive 30-day minimum runoff (DWF30) under 1.5 °C and 2.0 °C of global warming compared to the REF. The green and yellow rectangles indicate the location of regions susceptible to DWF07 and DWF30 under global warming. The green (yellow) lines indicate the regions in Cf (Bw) zone.
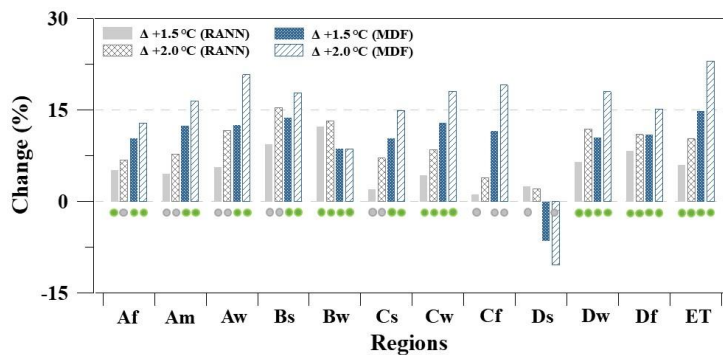
Figure 10: Relative changes in (a) annual mean runoff and (b) annual maximum runoff (MDF) for 12 climate zones derived from the MME of five GCMs under 1.5 °C and 2.0 °C of global warming compared to the REF. Green circles (gray circles) denote over 100 % (80 %) intermodel agreement.

Table 1: The climate zone classification method of Köppen using temperature and precipitation. (Tmin(max): monthly averaged minimum (maximum) temperature, Pmin: monthly averaged minimum precipitation, PANN: annual averaged precipitation, Psmin(smax): minimum (maximum) precipitation in the summer season, and Pwmin(wmax): minimum (maximum) precipitation in the winter season).

Type	Description	Criterion	Ratio of Area (%)
A	**Tropical climates**	$T_{min} \geq +18\ °C$	**17.2**
Af	Rainforest	$P_{min} \geq 60$ mm	5.8
Am	Monsoon	Not(Af) & $P_{min} \geq 100-P_{ANN}/25$	1.7
Aw	Savannah	Not(Af) & $P_{min} < 100-P_{ANN}/25$	9.7
B	**Arid climates**	$P_{ANN} < 10P_{th}$	**22.1**
BS	Steppe climate	$P_{ANN} > 5P_{th}$	4.6
BW	Desert climate	$P_{ANN} \leq 5P_{th}$	17.5
C	**Warm temperate climates**	$-3\ °C < T_{min} < +18\ °C$	**19.4**
Cs	Warm temperate climate with dry summer	$P_{smin} < P_{wmin}$ & $P_{wmax} > 3P_{smin}$ & $P_{smin} < 40$ mm	2.1
Cw	Warm temperate climate with dry winter	$P_{wmin} < P_{smin}$ & $P_{smax} > 10P_{wmin}$	10.5
Cf	Warm temperate climate without dry season	Neither Cs nor Cw	6.7
D	**Cold climates**	$T_{min} \leq -3\ °C$	**36.3**
Ds	Cold climate with dry summer	$P_{smin} < P_{wmin}$ & $P_{wmax} > 3P_{smin}$ & $P_{smin} < 40$ mm	1.8
Dw	Cold climate with dry winter	$P_{wmin} < P_{smin}$ & $P_{smax} > 10P_{wmin}$	19.7
Df	Cold climate without dry season	Neither Ds nor Dw	14.8
E	**Polar climates**	$T_{max} < +10\ °C$	**5.1**
ET	Tundra climate	$0\ °C \leq T_{max} < +10\ °C$	5.1
EF	Frost climate	$T_{max} < 0\ °C$	-

Table 2: List of the five selected GCMs used in this study.

635

No.	GCMs	Resolution (Lon.×Lat.)	Institute	Nation
1	bcc-csm1-1-m	1.125° × 1.125°	BCC	China
2	CanESM2	2.8125° × 2.8125°	CCCma	Canada
3	CMCC-CMS	1.875° × 1.875°	CMCC	Italy
4	CNRM-CM5	1.40625° × 1.40625°	CNRM-CERFACS	France
5	NorESM1-M	2.5°× 1.875°	NCC	Norway

640

Table 3: Global warming of 0.48 ℃, 1.5 ℃ and 2.0 ℃ under the RCP4.5 scenario for individual GCMs.

645

No.	GCMs	Reference periods (0.48 ℃)	Future periods (1.5 ℃)	Future periods (2.0 ℃)
1	bcc-csm1-1-m	1973 (1959-1988)	2013 (2006-2035)	2039 (2025-2054)
2	CanESM2	1983 (1969-1998)	2016 (2006-2035)	2031 (2017-2046)
3	CMCC-CMS	1996 (1982-2011)	2034 (2020-2049)	2052 (2038-2067)
4	CNRM-CM5	1988 (1974-2003)	2035 (2021-2050)	2056 (2042-2071)
5	NorESM1-M	1991 (1977-2006)	2041 (2027-2056)	2075 (2061-2090)

Table 4: Definitions of the hydroclimatic extreme indices, where 'i' and 'j' represent month and year, respectively.

Index name (label)	Index definition	Unit
Tropical nights (TR)	The number of days when $TN_{ij} > 20\,℃$	Days
Frost days (FD)	The number of days when $TN_{ij} < 0\,℃$	Days
Warm nights (TN90p)	The number of days when $TN_{ij} > TNref90$; here, TNref90 is the calendar day 90th percentile centered on a 5-day window for the reference period of individual GCMs	Days
Cold nights (TN10p)	The number of days when $TN_{ij} < TNref10$; here, TNref10 is the calendar day 10th percentile centered on a 5-day window for the reference period of individual GCMs	Days
Summer days (SU)	The number of days when $TX_{ij} > 25\,℃$	Days
Icing days (ID)	The number of days when $TX_{ij} < 0\,℃$	Days
Warm days (TX90p)	The number of days when $TX_{ij} > TXref90$; here, TXref90 is the calendar day 90th percentile centered on a 5-day window for the reference period of individual GCMs	Days
Cold days (TX10p)	The number of days when $TX_{ij} < TXref10$; here, TXref10 is the calendar day 10th percentile centered on a 5-day window for the reference period of individual GCMs	Days
Very wet day precipitation (P95)	Total precipitation when PR_{ij} exceeds the 95th percentile of the wet day precipitation in the reference period of individual GCMs	Mm
Extreme wet day precipitation (P99)	Total precipitation when PR_{ij} exceeds the 99th percentile of the wet day precipitation in the reference period of individual GCMs	Mm
Annual maximum precipitation (PX1D)	The maximum 1-day precipitation	Mm
Maximum 2-day precipitation (PX2D)	The maximum consecutive 2-day precipitation	Mm
Maximum 3-day precipitation (PX3D)	The maximum consecutive 3-day precipitation	Mm
Maximum 5-day precipitation (PX5D)	The maximum consecutive 5-day precipitation	Mm
Minimum 7-day runoff (DWF07)	The minimum of consecutive 7-day runoff	Mm
Minimum 30-day runoff (DWF30)	The minimum of consecutive 30-day runoff	Mm
Annual maximum runoff (MDF)	The maximum daily runoff	Mm

Table 5: Plots of the percentage changes in the climate extreme indices in response to the additional 0.5 °C warming in the climate zones over Asia, where '*' and '' represent significance at the 80 and 100 % agreement levels, respectively.**

	FD	ID	SU	TR	TX10P	TN10P	TX90P	TN90P	PANN	PX1D	PX2D	PX3D	PX5D	P95	P99	RANN	MDF	DWF07	DWF30
Af	-	-	-	**	**	**	**	**	*	**	**	**	**	*		*			
Am	-	-	**	**	**	**	**	**	*	*	**	**	**	**	**	*	*		
Aw	-	-	**	**	**	**	**	**	**	*	*	*	*	*	*	**	*		
BS	**	**	**	**	**	**	**	**	**	*	*	**	**	**	*	**	*		
BW	**	**	**	**	**	**	**	**		*	*	*	*		*		*		
Cs	**	**	**	**	**	**	**	**		*	*						*		
Cw	**	**	**	**	**	**	**	**	**	*	**	**	*	**	*	**	**		
Cf	**	**	**	**	**	**	**	**	*	*	**	**	**	*	**	*	**		
Ds	**	**	**	**	**	**	**	**		*	*	*	*				*		
Dw	**	**	**	**	**	**	**	**	**	**	**	**	**	**	**	**	**		
Df	**	**	**	**	**	**	**	**	**	**	**	**	**	**	**	**	**		
ET	**	**	**	-	**	**	**	**	**	**	**	**	**	**	**	**	**		*

-20 -15 -10 -8 -6 -4 -2 0 2 4 6 8 10 15 20 (%)